
Princeton Plasma Physics Laboratory

PPPL-

PPPL-



Prepared for the U.S. Department of Energy under Contract DE-AC02-09CH11466.

Princeton Plasma Physics Laboratory

Report Disclaimers

Full Legal Disclaimer

This report was prepared as an account of work sponsored by an agency of the United States Government. Neither the United States Government nor any agency thereof, nor any of their employees, nor any of their contractors, subcontractors or their employees, makes any warranty, express or implied, or assumes any legal liability or responsibility for the accuracy, completeness, or any third party's use or the results of such use of any information, apparatus, product, or process disclosed, or represents that its use would not infringe privately owned rights. Reference herein to any specific commercial product, process, or service by trade name, trademark, manufacturer, or otherwise, does not necessarily constitute or imply its endorsement, recommendation, or favoring by the United States Government or any agency thereof or its contractors or subcontractors. The views and opinions of authors expressed herein do not necessarily state or reflect those of the United States Government or any agency thereof.

Trademark Disclaimer

Reference herein to any specific commercial product, process, or service by trade name, trademark, manufacturer, or otherwise, does not necessarily constitute or imply its endorsement, recommendation, or favoring by the United States Government or any agency thereof or its contractors or subcontractors.

PPPL Report Availability

Princeton Plasma Physics Laboratory:

<http://www.pppl.gov/techreports.cfm>

Office of Scientific and Technical Information (OSTI):

<http://www.osti.gov/bridge>

Related Links:

[U.S. Department of Energy](#)

[Office of Scientific and Technical Information](#)

[Fusion Links](#)

Neoclassical Toroidal Viscosity in Perturbed Equilibria with General Tokamak Geometry

Nikolas C. Logan, Jong-Kyu Park, Kimin Kim, Zhirui Wang, John W. Berkery¹¹

*Plasma Physics Laboratory, Princeton University, Princeton, New Jersey 08543,
USA*

¹*Department of Applied Physics and Applied Mathematics,
Columbia University, New York, New York 10027,
USA*

(Dated: October 11, 2013)

This paper presents a calculation of neoclassical toroidal viscous (NTV) torque independent of large-aspect-ratio expansions across kinetic regimes. The Perturbed Equilibrium Nonambipolar Transport (PENT) code was developed for this purpose, and is compared to previous combined regime models as well as regime specific limits and a drift kinetic δf guiding center code. It is shown that retaining general expressions, without circular large-aspect-ratio or other orbit approximations, can be important at experimentally relevant aspect ratio and shaping. The superbanana plateau, a kinetic resonance effect recently recognized for its relevance to ITER, is recovered by the PENT calculations and shown to require highly accurate treatment of geometric effects.

I. INTRODUCTION

The toroidal rotation of magnetically confined plasma in tokamaks has important stabilizing effects, and the control of this rotation is of great importance in designing the next generation of fusion experiments such as ITER and future reactors. It has long been known, however, that magnetic nonaxisymmetries in tokamaks as small as $\delta B/B \approx 10^{-4}$ can have significant effects on the rotation as increased neoclassical toroidal viscosity (NTV) leads to increased toroidal flow damping¹⁻³. Recently, these effects have received much attention as a potential method of rotation and stability control using applied nonaxisymmetric perturbations to alternately decrease or increase the plasma rotation⁴⁻⁶. It is thus critical to develop models that can accurately predict the effects of non-axisymmetry in tokamaks on toroidal rotation.

When magnetic field strength cannot be expressed as a function of a flux surface label ψ and distance along a field line l , such that $B = B(\psi, l)$, the action $J = \oint dl M v_{\parallel}$ of a particle with mass M and velocity parallel to the field lines v_{\parallel} is not conserved on flux surfaces and the particle experiences radial drifts across flux surfaces⁷. This radial transport depends on the particle species and is not intrinsically ambipolar. The resulting nonambipolar transport produces radial currents that in turn produce $\mathbf{J} \times \mathbf{B}$ toroidal torque, where \mathbf{J} is the current density. This torque from nonambipolar transport in tokamaks is called neoclassical toroidal viscous (NTV) torque, and been observed to be the dominant influence on rotation in the presence of the non-resonant nonaxisymmetric perturbations^{3,4,8}.

Theoretical predictions of the NTV torque, however, are nontrivial due to detailed phase space structure that is dependent on different particle orbits, precessions, and collisions. A number of theories have been developed in limited regimes to simplify or ignore one or more such dependencies. The effects of passing and trapped particles are studied separately and various trapped particle effects are also studied separately in many different collisionality (ν) regimes including the $1/\nu$ regime, $\nu_{-}\sqrt{\nu}$ regime, superbanana-plateau regime, and superbanana regime, or combined using approximate connection formulae assuming pitch-angle collisions⁹. Recognizing the practical importance of overlapping between the regimes, a combined NTV model has been developed using a Krook collision operator but including all bounce and precession orbits¹⁰. The combined theory, valid across the range of kinetic regimes, is fully implemented in general aspect ratio and shaped plasmas by the Perturbed

Equilibrium Nonambipolar Transport (PENT) code developed in conjunction with the Ideal Perturbed Equilibrium Code (IPEC)^{11,12} and initial NTV torque predictions are presented in the following sections.

This paper is organized as follows. Section II outlines the combined NTV theory, including a complete treatment of pitch angle dependencies in the bounce frequency, precession frequency and perturbed action. The validity of previous circular large-aspect-ratio and orbit approximations for trapped particles is discussed in Sec. III. Finally, the generalized PENT computation is shown to recover expected limiting behavior for superbanana plateau more precisely compared to the previous approximations in Sec. IV. Section V contains concluding remarks.

II. COMBINED NTV THEORY

In this section we derive an analytical form of the toroidal torque that arises from neoclassical ambipolar transport, often referred to as neoclassical toroidal viscous (NTV) torque, valid across kinetic regimes. The results reproduce those previously developed in a reduced large-aspect-ratio (RLAR) limit^{10,13}, but are given here in their most general form. The derivation thus serves an important purpose in orienting the reader to the geometry dependent quantities and their ultimate role in the NTV torque. The structure of the derivation will be as follows: First, a general form for toroidal torque in magnetic coordinates is expanded using an anisotropic perturbed pressure tensor and linear expansion of the non-axisymmetric equilibrium quantities. Next, the torque is written in its phase space representation and closed using the first order linearized drift-kinetic equation. The zeroth order drift-kinetic solution, a Maxwellian distribution function, is used in the final step to connect to familiar offset rotation physics^{4,14}.

The general relation, given by Boozer¹⁵, for toroidal torque in a closed magnetic confinement device is,

$$T_\varphi = \int d^3x \left(\frac{\partial \mathbf{x}}{\partial \varphi} \cdot \nabla \cdot \overleftrightarrow{\Pi} \right) = -\frac{1}{2} \sum_{ij} \int d^3x \frac{\partial g_{ij}}{\partial \varphi} \Pi^{ij}, \quad (1)$$

where g is the coordinate metric tensor and $\overleftrightarrow{\Pi}$ is the pressure tensor with equilibrium $\overleftrightarrow{\Pi} = 0$ on magnetic surfaces. We now introduce a simple tensor pressure, in which the parallel and perpendicular pressures are distinct $\overleftrightarrow{\Pi} = (\delta p_{\parallel} - \delta p_{\perp}) \hat{b}\hat{b} + \delta p_{\perp} \overleftrightarrow{\mathbf{I}}$ ^{15,16}. We

define our field in Clebsch representation with magnetic coordinates $(\psi, \vartheta, \alpha)$ such that $\mathbf{B} = \nabla\alpha \times \nabla\psi$ where ψ is the poloidal flux and the poloidal angle is defined as relating the toroidal angle α to the standard toroidal angle $\phi = \alpha + q(\psi)\vartheta$ with the safety factor q ^{17,18}.

This gives,

$$\hat{b}b^{ij} = \left(\frac{\frac{\partial \mathbf{x}}{\partial \vartheta} \cdot \frac{\partial x^i}{\partial \mathbf{x}}}{\mathcal{J}B} \right) \left(\frac{\frac{\partial \mathbf{x}}{\partial \vartheta} \cdot \frac{\partial x^j}{\partial \mathbf{x}}}{\mathcal{J}B} \right) = \frac{\delta_{ij}^{\vartheta}}{(\mathcal{J}B)^2},$$

and,

$$g_{\vartheta\vartheta} = \frac{\partial \mathbf{x}}{\partial \vartheta} \cdot \frac{\partial \mathbf{x}}{\partial \vartheta} = (\mathcal{J}B)^2,$$

where we have introduced the Jacobian $\mathcal{J}^{-1} = \nabla\psi \times \nabla\vartheta \cdot \nabla\alpha$. The torque equation is thus expanded to,

$$T_\varphi = -\frac{1}{2} \sum_{ij} \int d^3x \frac{(\delta p_{\parallel} - \delta p_{\perp})}{(\mathcal{J}B)^2} \frac{\partial}{\partial \varphi} (\mathcal{J}B)^2 + \delta p_{\perp} \overleftrightarrow{\mathbf{I}} \frac{\partial g_{ij}}{\partial \varphi}, \quad (2)$$

which can be further simplified noting the identities $\overleftrightarrow{\mathbf{I}} = g^{ij}$ and $\sum_{ij} g^{ij} \partial g_{ij} / \partial \varphi = (2/\mathcal{J}) \partial \mathcal{J} / \partial \varphi$,

$$T_\varphi = - \int d^3x (\delta p_{\parallel} - \delta p_{\perp}) \frac{1}{B} \frac{\partial B}{\partial \varphi} + \delta p_{\parallel} \frac{1}{\mathcal{J}} \frac{\partial \mathcal{J}}{\partial \varphi}. \quad (3)$$

The equilibrium Jacobian and magnetic field are assumed axisymmetric with small non-axisymmetric perturbations. To first order, these perturbed quantities are the change in flux surface arc-length $\mathcal{J} = \mathcal{J}(\psi, \vartheta)(1 + \nabla \cdot \boldsymbol{\xi})$ and the Lagrangian perturbed field $\mathbf{B} = \mathbf{B}(\psi, \vartheta) + \delta \mathbf{B}(\psi, \vartheta, \varphi)$. This gives,

$$T_\varphi = - \int d^3x \left[(\delta p_{\parallel} - \delta p_{\perp}) \frac{1}{B} \frac{\partial \delta B}{\partial \varphi} + \delta p_{\parallel} \frac{\partial}{\partial \varphi} (\nabla \cdot \boldsymbol{\xi}) \right], \quad (4)$$

where the non-perturbed quantities are all the zeroth order axisymmetric values and the integrand -a second order quantity- represents the toroidal torque in a non-axisymmetric perturbed equilibrium.

Much of the important physics associated with NTV torque is a result of kinetic effects, thus far absent from this derivation. Inserting the phase space integral definitions of each perturbed pressure, $\delta p_{\parallel} = \int d^3v M v_{\parallel}^2 f_1$ and $\delta p_{\perp} = \int d^3v M v_{\perp}^2 f_1 / 2$ where f_1 is the perturbed distribution function, into (4) and converting to energy coordinates ($E = Mv^2/2, \mu = Mv_{\perp}^2/2B$) we arrive at a more insightful form of the toroidal torque,

$$T_\varphi = -\frac{4\pi}{M^2} \int d^3x d\mu dE f_1 \frac{\mathcal{J}BM}{v_\parallel} \left[(2E - 3\mu B) \frac{\partial}{\partial \varphi} \frac{\delta B}{B} + (2E - 2\mu B) \frac{\partial}{\partial \varphi} (\nabla \cdot \boldsymbol{\xi}) \right]. \quad (5)$$

Note that the second term in the bracket above corresponds to the arc-length change in the perturbed equilibrium, but is often ignored in the large-aspect-ratio NTV approximation with $\mu B \approx E$ for trapped particles.

At this point, it is necessary to solve for the perturbed distribution function. An appropriate model for the ideal perturbed equilibrium is the bounce averaged, first order drift-kinetic equation¹⁹. Explicitly, the drift-kinetic equation,

$$\mathbf{v}_\parallel \cdot \nabla f_{i1} + \mathbf{v}_{di}^\alpha \frac{\partial f_{i1}}{\partial \alpha} - C_{i1} f_{i1} = -\mathbf{v}_{di}^\psi \frac{\partial f_{i0}}{\partial \psi}, \quad (6)$$

becomes,

$$\begin{aligned} \left\langle -2\pi i(\ell - \sigma n q) \frac{\partial h}{\partial \vartheta} v_\parallel \frac{\mathbf{B}}{B} \cdot \nabla \vartheta - 2\pi i n \mathbf{v}_{di} \cdot \nabla \alpha + \nu_i \right\rangle \delta f_\ell \\ = \left\langle -\mathcal{P}_\ell^{-1} \mathbf{v}_{di} \cdot \nabla \psi \frac{\partial f_{i0}}{\partial \psi} \right\rangle, \end{aligned} \quad (7)$$

where the subscript i refers to the particle species, numeric subscripts refer to small gyro-radius ordering, \mathbf{v}_d is the the drift velocity, and a simple Krook collision operator $Cf = -\nu_i f$ is assumed. The angular brackets in Eq. (7) refer to the bounce average defined by $\langle A \rangle_b \equiv \oint (Adl/v_\parallel) / \oint (dl/v_\parallel) = \frac{\omega_b}{2\pi} \oint d\vartheta A \mathcal{J}B/v_\parallel$ with the bounce frequency $\omega_b \equiv 2\pi / \oint d\vartheta \mathcal{J}B/v_\parallel$. Note that the parallel electric field term for electrons has not been included in Eq. (6) since the Ware pinch effect is annihilated by the subsequent bounce averaging. The bounce average isolates the non-axisymmetry driven perturbation to the distribution²⁰, and is well defined only for those species with closed orbits such that,

$$f_{i1} = f_{i1}(\mathbf{v}, \psi) e^{-i2\pi n \alpha} e^{-i2\pi(\ell - \sigma n q)h(\mathbf{v}, \vartheta)} = \delta f_\ell \mathcal{P}_\ell. \quad (8)$$

Here, $\sigma = 1(0)$ for passing(trapped) particles, $h(\mathbf{v}, \vartheta) = \left(\int_0^\vartheta d\theta \mathcal{J}B v_d^\alpha / v_\parallel \right) / \oint d\theta \mathcal{J}B v_d^\alpha / v_\parallel$ is the α -phase of a particle as a function of ϑ , n is the toroidal mode number of the non-axisymmetric perturbations, $\ell - \sigma n q$ is the number of toroidal transits after which the particle

returns to an original point in space, and the phase-factor $\mathcal{P}_\ell = e^{-i2\pi(\ell - \sigma n q)h}$ contains all the ϑ dependence. In writing Eq. (7) we have assumed decoupling between ℓ -species, which can be strictly proved in the circular large-aspect-ratio limit with $\omega_E \gg \omega_D$.

The drift velocity in Eq. (7) is the sum of gradient, electric, and curvature drifts,

$$\mathbf{v}_d = \frac{\mathbf{B}}{eB^2} \times \left(\mu \nabla B + e \nabla \Phi + M v_\parallel^2 \frac{[(\mathbf{B} \cdot \nabla) \mathbf{B}]}{B^2} \right) \quad (9)$$

$$= \frac{v_\parallel}{B} \nabla \times (\rho_\parallel \mathbf{B}) - \frac{v_\parallel}{B^3} \rho_\parallel [\mathbf{B} \cdot (\nabla \times \mathbf{B})] \mathbf{B}, \quad (10)$$

where e is the charge of the particle species, Φ is the electric potential, and we have defined $\rho_\parallel \equiv M v_\parallel / e B$. In writing Eq. (10) from (9) we used the conservation of total energy (\mathcal{E}), $\nabla \mathcal{E} = 0 = M v_\parallel \nabla v_\parallel + \mu \nabla B + e \nabla \Phi$, and a few vector formulae.

Inserting Eqs. (8) and (10) into Eq. (6), we obtain,

$$[-i\omega_b(\ell - nq) - in(\omega_E + \omega_D) + \nu_i] \delta f_\ell = \frac{\omega_b}{2\pi e} \frac{\partial \delta J_{-\ell}}{\partial \alpha} \frac{\partial f_{i0}}{\partial \psi}. \quad (11)$$

Here we have defined the electric and magnetic precession frequencies as,

$$\omega_E \equiv -2\pi \frac{\partial \Phi}{\partial \psi}, \quad (12)$$

and,

$$\omega_D \equiv 2\pi \left\langle \left(E - \frac{3}{2} \mu B \right) \frac{2}{eB} \frac{\partial B}{\partial \psi} + (E - \mu B) \frac{2}{e\mathcal{J}} \frac{\partial \mathcal{J}}{\partial \psi} \right\rangle_b, \quad (13)$$

as well as the variation in the action,

$$\begin{aligned} \frac{\partial \delta J_{\pm \ell}}{\partial \alpha} &\equiv M \int d\vartheta \mathcal{P}_\ell^{\pm 1} \delta (v_\parallel \mathcal{J} B), \quad (14) \\ &= \oint d\vartheta \frac{\mathcal{J} B}{v_\parallel} \mathcal{P}_\ell^{\pm 1} \left[(2E - 3\mu B) \frac{1}{B} \frac{\partial \delta B}{\partial \alpha} + \right. \\ &\quad \left. (2E - 2\mu B) \frac{1}{\mathcal{J}} \frac{\partial}{\partial \alpha} \nabla \cdot \boldsymbol{\xi} \right]. \quad (15) \end{aligned}$$

Again, the bounce-averaging process has eliminated the $\partial/\partial\vartheta$ terms from $v_{di}^{\alpha, \psi}$ normally associated with axisymmetric neoclassical transport. It should be noted that by doing so, we make the momentum transport solution inherently a nonlocal quantity. The solution (11) is valid for both trapped and passing particles, and contains contributions from curvature drifts and the perturbed arc-length in ω_D and δJ_ℓ often ignored in large-aspect-ratio

approximations^{10,21}. The dependencies on aspect ratio and shaping enter the torque calculation through these terms.

The bounce averaged torque is given by inserting the non-axisymmetry driven perturbed distribution (11) in the phase space integral form of the toroidal torque (5),

$$T_\varphi = \frac{1}{eM^2} \int d\psi d\alpha d\mu dE \mathcal{R}_\ell \left| \frac{\partial \delta J_\ell}{\partial \alpha} \right|^2 \frac{\partial f_{i0}}{\partial \psi}. \quad (16)$$

Here, the resonant operator $\mathcal{R}_\ell = \omega_b / \{i[(\ell - \sigma n q)\omega_b - n(\omega_E + \omega_D)] - \nu_i\}$ contains the important bounce harmonic resonance physics^{10,13} discussed extensively in the following sections. The well known offset rotation is explicitly included in the resonant operator when introducing the zeroth order drift-kinetic solution Maxwellian,

$$f_{i0} = \frac{N}{(2\pi T/M)^{3/2}} \exp\left(-\frac{\mathcal{E} - e\Phi}{T}\right), \quad (17)$$

where N is the species density, T is the species temperature and the density, temperature and electric potential are all functions of the flux variable ψ only. The derivative of this distribution with respect to ψ is taken at constant total energy,

$$\frac{\partial f_{i0}}{\partial \psi} \Big|_{\mathcal{E}} = -\frac{ef_0}{2\pi T} \left[\omega_E + \omega_{*N} + \omega_{*T} \left(\frac{E}{T} - \frac{3}{2} \right) \right]. \quad (18)$$

Placing Eq. (18) in Eq. (16), assuming perturbations of the form $\delta A \sim e^{in\alpha}$, and making a final conversion to normalized energy coordinates ($x = E/T$, $\Lambda = \mu B_0/E$) gives,

$$T_\varphi = -\frac{n^2 R_0}{\sqrt{\pi} B_0} \int d\psi NT \int d\Lambda \bar{\omega}_b |\delta \bar{J}_\ell|^2 \int dx \mathcal{R}_{T\ell}, \quad (19)$$

with,

$$\mathcal{R}_{T\ell} = \frac{[\omega_\varphi + \omega_{*T}(x - \frac{5}{2})] x^{5/2} e^{-x}}{i[(\ell - \sigma n q)\omega_b + n(\omega_E + \omega_D)] - \nu_i}. \quad (20)$$

Here, B_0 refers to the magnitude of the magnetic field on axis and both $\bar{\omega}_b = \omega_b R_0 / \sqrt{2xT/M}$ and $\delta \bar{J}_\ell^2 = \delta J_\ell^2 / 2xTM R_0^2$ are unit-less quantities. Note that this expression is valid for a single, Maxwellian particle species, and should be summed over species if more than one significantly contributes to the torque. The toroidal rotation frequency has been included

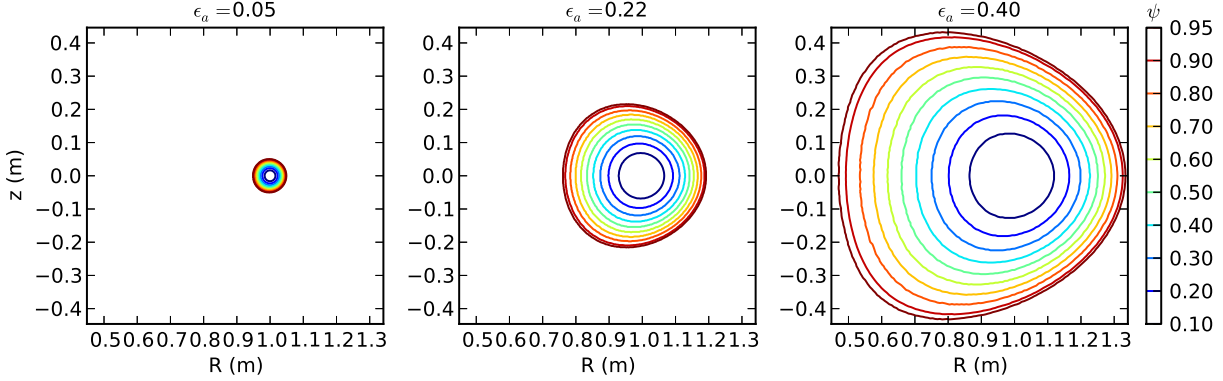


Figure 1. Solov'ev equilibria with $\kappa = 1$, $q_0 = 2.2$, $B_0 = 1\text{T}$ and $R_0 = 1\text{m}$. The equilibria have limited shaping, and approach the circular limit for $\epsilon_a \rightarrow 0$.

in Eq. (20) using radial force balance neglecting poloidal rotation $\omega_\varphi = \omega_E + \omega_{*T} + \omega_{*N}$ ^{14,22} in order to explicitly show that the resonant operator -and ultimately the torque on a given magnetic surface- is proportional to the rotation with an offset value.

The result is left in its complex form since the imaginary component of the torque has been shown to be proportional to the perturbed kinetic energy, $2n\delta W_k$ ¹³. The calculations at the heart of PENT, therefore, is physically equivalent to those done by stability codes MARS-K^{23,24}, MISK^{25,26}, and MISHKA²⁷ in the case of static, marginally stable ($|T_\varphi| \ll |2n\delta W_k|$) resistive wall modes.

The final form given by Eqs. (19) and (20) represents an expression for the toroidal torque and perturbed kinetic energy driven by non-axisymmetric perturbations to an axisymmetric equilibrium valid across all kinetic regimes. Although it uses a simplified collision operator, it contains important bounce harmonic resonance physics that can dominate the torque in experimental devices. Here, in its complete form, the resonance operator is a function of both energy and pitch (x, Λ), such that geometric shaping or low aspect ratio effects may influence the NTV through sensitive resonance conditions. Capturing these kinetic resonances in the true geometric shaping of modern experiments is an important computational task, and is the subject of the following section.

III. PITCH ANGLE DEPENDENCIES AND GEOMETRIC EFFECTS

The PENT code has been developed to calculate the NTV torque from Eqs. (19) and (20), without any geometric simplifications in the bounce frequencies, precession frequencies or perturbed action. The combined theory presented in Ref.¹⁰ used circular large-aspect-ratio approximations and further removed pitch (Λ) dependence of bounce and magnetic precession frequencies,

$$\omega_b \approx \sqrt{\frac{\epsilon x \Lambda}{2}} \omega_t \frac{\pi}{K(k)} \approx \frac{\pi}{4} \sqrt{\frac{\epsilon}{2}} \omega_t \sqrt{x}, \quad (21)$$

$$\omega_D \approx \frac{q^3 \Lambda}{\epsilon} x \left[\frac{E(k)}{K(k)} - \frac{1}{2} \right] \approx \frac{q^3 \omega_t^2}{4\epsilon \omega_g} x. \quad (22)$$

Here ϵ is the inverse aspect ratio, ω_t is the transit frequency, ω_g is the gyro-frequency, K and E are the complete elliptic integrals of the first and second kind respectively and their argument is $k = \sqrt{(1 - \Lambda + \epsilon \Lambda) / (2\epsilon \Lambda)}$. The reduced large-aspect-ratio (RLAR) approximations on the far right correspond approximately to the Λ -averaged circular larger-aspect-ratio approximations for trapped particles that they follow¹⁰. In practice, these were designed to separate the computationally demanding double integration in (x, k) space of the resonant operator assuming $\omega_E \gg \omega_D$ in most applications. The PENT code, in contrast, solves the full bounce averaged expressions for both frequencies throughout the phase space populated by passing and trapped particles.

The large-aspect-ratio approximation can deteriorate as the aspect ratio approaches unity and/or shaping is introduced into the plasma equilibrium. For demonstration, the NTV torque from trapped ions as calculated using the full and RLAR formalisms in an aspect ratio scan of Solov'ev equilibria is presented here. The Solov'ev equilibria are analytic solutions of the Grad-Shafranov equation for which the current and pressure profiles are fully defined by the elongation κ , safety factor on axis q_0 , field on axis B_0 , major radius R_0 and inverse aspect ratio $\epsilon_a = a/R_0$ where a is the minor radius^{28,29}. The equilibria used here have common parameters $\kappa = 1$, $q_0 = 2.2$, $B_0 = 1\text{T}$, $R_0 = 1\text{m}$, and are henceforth referred to solely by their inverse aspect ratio. Figure 1 shows flux surfaces for three such equilibria. Note that the Solov'ev solution is defined for $\epsilon_a < 0.5$, as shaping at low aspect ratio weights the boundary towards the $R = 0$ vertical axis.

The ratio of the NTV torque calculated using the full calculation in PENT to the RLAR approximation across a scan of the inverse aspect ratio is presented in Fig. 2. In each case, the

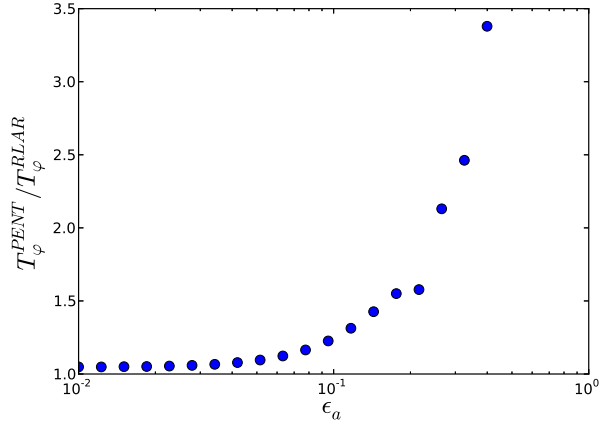


Figure 2. The ratio of NTV torque as calculated by PENT and the RLAR approximation approaches unity as the inverse aspect ratio ϵ_a approaches 0, but becomes aggressively large ϵ_a approaches its maximum value of 0.5.

Solov’ev equilibrium is perturbed in IPEC using an applied 1 Gauss non-resonant $m/n = 2/1$ mode on the outermost flux surface where m and n are the poloidal and toroidal harmonics respectively. The electron and deuterium ion density and temperature profiles, as well as the electric precession profiles are set constant as $n(\psi) = n_0(1 - 0.7\psi)$, $P(\psi) = P_0(1 - \psi)$ and $\omega_E = \omega_{E0}(1 - \psi)$ with on-axis values $n_0 = 1.12 \times 10^{-20} \text{m}^{-3}$, $P_0 = 2.33 \times 10^4 \text{Pa}$, and $\omega_{E0} = 0.63 \text{kHz}$. The collisionality in this case is near the $1/\nu$ collisionality regime⁹. As the inverse aspect ratio approaches 0, the equilibria become cylindrical and the RLAR agrees well with the PENT calculation. At larger ϵ_a , however, both the large-aspect-ratio and the circular approximations begin to break and the RLAR torque significantly underestimates the total torque predicted by the combined theory without geometric simplification.

A closer look at the simplifications (21) and (22) in the Solov’ev aspect ratio scan provides insight into the physics missed in the RLAR approximation. Figure 3 shows the bounce and precession frequencies in the RLAR and circular large-aspect-ratio approximations compared to the full bounce-averaged values for all trapped particles on the $\psi = 0.66$ surface for representative large and low aspect ratio Solov’ev equilibria. Note that the RLAR approximation ignores strong Λ -dependencies. In a large-aspect-ratio case such as $\epsilon_a = 0.05$, this reduction can be valid for ω_b in average although a subtle interplay between the disappearing ω_b and potentially large $|\delta J_\ell|^2$ for weakly trapped particles is not accounted for. As ϵ_a increases, ω_b calculated with the full geometry can largely differ from the large-aspect-ratio and thus

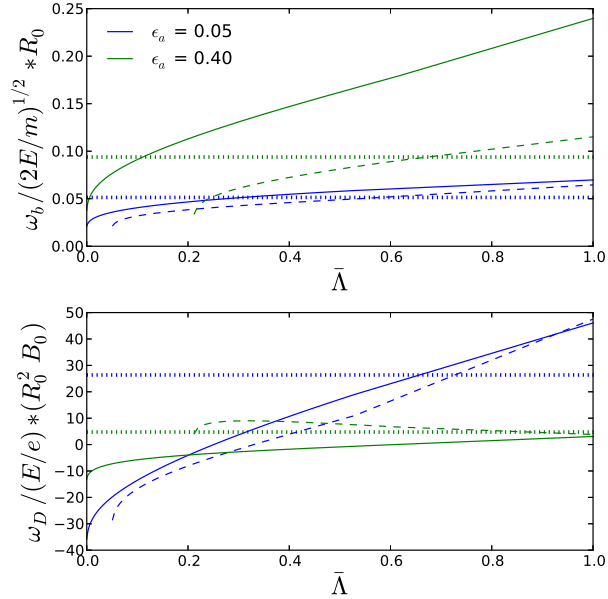


Figure 3. The pitch angle dependent profiles of the bounce (top) and magnetic precession (bottom) frequencies in PENT (solid), the circular large-aspect-ratio approximation (dashed) and the RLAR approximation (dotted) for trapped ions on the $\psi = 0.66$ surface of two Solov’ev equilibria. The normalized axis $\bar{\Lambda} = (\Lambda - B_0/B_{max}) / (B_0/B_{min} - B_0/B_{max})$ increases from 0 at the trapped-passing boundary to 1 at the deeply trapped limit.

further from the RLAR approximation. The deviation at higher ϵ_a is also severe for ω_D . The RLAR approximation ignores the sign change between the deeply and marginally trapped species and thus will be unable to capture a limiting behavior for $\omega_E \rightarrow \omega_D$, and it is shown that even the circular large-aspect-ratio approximation can become significantly incorrect for ϵ_a approaching its maximum. The next section looks in more detail at how retaining the Λ dependence of these profiles can play an important role in describing resonance particles precisely.

IV. PITCH ANGLE RESONANCE AND THE SUPERBANANA PLATEAU

Bounce-harmonic resonant (BHR) particles, satisfying $(\ell - \sigma nq)\omega_b - n(\omega_E + \omega_D) \approx 0$, have been shown to dominate the nonambipolar transport and resulting toroidal torque in kinetic regimes relevant to present day and future tokamaks^{10,30,31}. The precision of the ω_b and ω_D representation in (x, Λ) becomes critical when $\nu_i \rightarrow 0$ since then the integration of

the resonant operator becomes stiff and essentially produces a δ function for BHR particles.

One such regime, the so-called Superbanana Plateau (SBP)^{5,21,32–34}, is expected when ω_E is as small as ω_D and $\nu_i \rightarrow 0 < |\omega_D|$. An analytic expression for SBP NTV characterized by precession resonances ($\ell = 0$ BHR) has been derived in Ref.²¹ using circular large-aspect-ratio approximations for ω_b , ω_D , and δJ as well as a Krook collision operator (known to be accurate in this regime^{35,36}).

The analytical SBP approximation requires an effective collisionality less than the precession frequency away from the kinetic resonance, whereas an effective collision frequency much larger than the precession frequency results in $1/\nu$ regime behavior³⁷. Here, the effective collisionality will be identified by the normalized parameter $\nu_* = \nu_i Rq / (\epsilon^{3/2} v_{th})$, where $v_{th} = \sqrt{2T/M}$ is the species thermal velocity.

Figure 4 shows the torque as calculated in PENT and the RLAR approximation as a function of ν_* across the SBP and $1/\nu$ regimes for a perturbed Solov’ev equilibrium consistent with those in Sec. III and $\epsilon_a = 0.3$. The torque is calculated over the entire plasma. The PENT profiles peak near the rational surface at $\psi \sim 0.66$, and $\nu_*(\psi = 0.66)$ is used for the axis in Fig. (4). Only the precession resonances ($\ell = 0$ species) are taken into account for consistency with²¹, and small $\omega_E \sim \mathcal{O}(\omega_D)$ is chosen to eventually reach SBP limits and to compare with the analytic SBP calculation. One can see that the RLAR and PENT torque calculations agree in the high-collisionality limit, but the RLAR calculation fails to capture the plateau behavior expected at low collisionality. On the other hand, it is also shown that the PENT plateau torque is a factor of ~ 4 lower than the SBP calculation. In order to compare these semi-analytic results with a more fundamental computation, the drift-kinetic δf guiding-center particle code, POCA^{30,34}, is used to calculate the NTV torque in the same Solov’ev targets as shown in Fig. 4. The PENT results agree best with the POCA results, indicating that the phase space structure of the BHR condition contains important details beyond the circular large-aspect-ratio approximations.

The superbanana plateau captured in these PENT computations is a result of BHR particles dominating the torque with the resonance near the precession frequency zero crossing in Λ . The analytic derivation of the SBP flux (and thus torque) relies on this resonance in Λ , approximating the real part of the resonant operator (20) as a delta function in pitch angle in the limit $n(\omega_D + \omega_E) \gg \nu$ ²¹. It is emphasized in Ref.²¹ that the existence of the plateau is a consequence of treating this singularity in the resonance operator independent

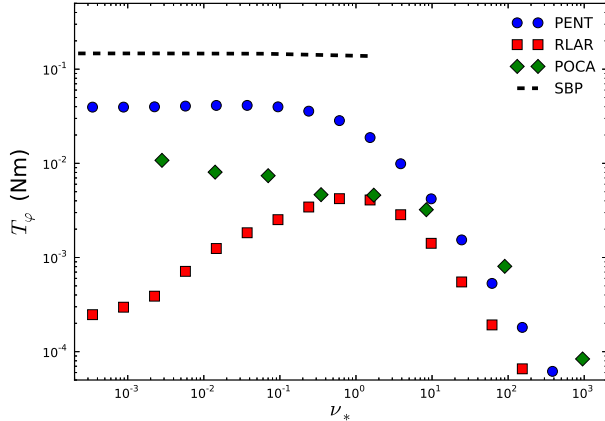


Figure 4. NTV torque across SBP, $1/\nu$, and intermediate regimes as computed in PENT with full pitch angle dependent ω_b , ω_D , and δJ (blue circles) compared to the RLAR approximation (red squares) shows the PENT calculation recovers the collisionality independence of the superbanana plateau. A SBP limit circular large-aspect-ratio calculation (dashed line) and POCA δf particle simulation (green diamonds) are also shown.

of geometric details. Therefore, it is not surprising that the RLAR approximation failed to capture SBP behavior³² when this singularity in Λ is not included. The analytic SBP calculation predicts the plateau behavior, but can be incorrect quantitatively in general equilibria due to the sensitive geometric dependency of ω_D .

It should be noted that global particle simulations by FORTEC-3D code did not show the SBP limiting behavior³². It is possible that particles can be decorrelated quickly from the sharp SBP resonant conditions in the course of radial transport or that the superbanana regime can play more important roles in low collisionality than theoretically predicted. This is beyond the scope of this paper but is clearly another important subject that a global simulation can test in the future.

Figure 5 shows the pitch angle dependence of the combined theory NTV torque in PENT smoothly transition from the isotropic $1/\nu$ regime toward the delta function resonance behavior at the BHR condition for moderately trapped particles near the precession null in the SBP limit. The amplitude of the delta function like resonance in the SBP depends on its location in Λ , which is highly dependent on the details of ω_D . Through changes in the resonant pitch condition, the curvature drift emphasized in Sec. II has a large effect on the ultimate value of the plateau torque calculated in PENT. This, combined with

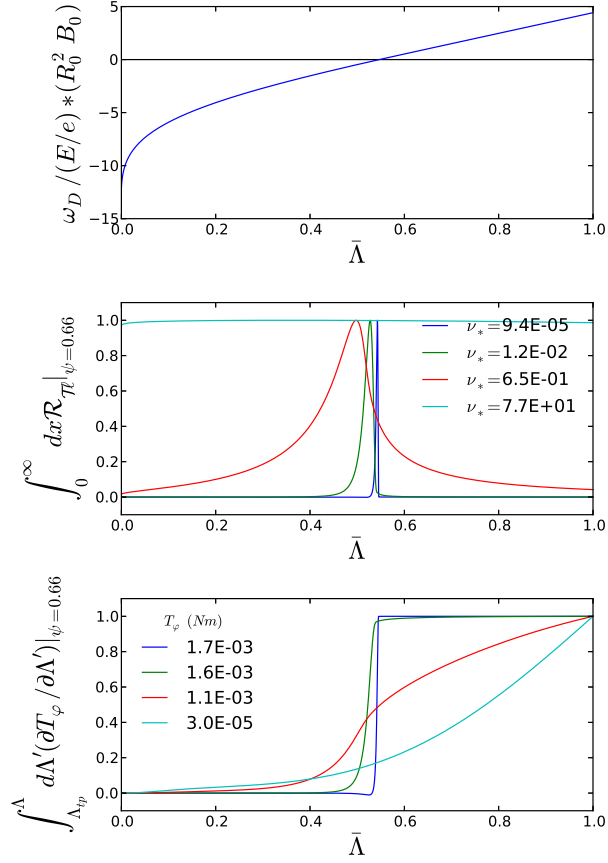


Figure 5. The magnetic precession (top), normalized energy integrated resonant operator (middle) and normalized cumulative integral torque (bottom) on the $\psi = 0.66$ surface for 4 collisionalities spanning the SBP and $1/\nu$ regimes. The torque is 1.7×10^{-3} , 1.6×10^{-3} , 1.1×10^{-3} , and 3×10^{-5} Nm for ν_* values of 9.4×10^{-5} (dark blue), 1.2×10^{-2} (green), 6.5×10^{-1} (red), and 7.7×10^1 (light blue) respectively. Sensitivity to precession resonances in Λ becomes more pronounced as the collisionality is reduced. The Λ resonance clearly dominates the NTV torque in the low collisionality limit.

the generalization of the perturbed action to include changes in the arc-length, brings the combined NTV torque plateau down and into better agreement with the more general and computationally expensive POCA results.

V. CONCLUSIONS

This paper presents a complete form of the NTV torque in perturbed equilibria valid across kinetic regimes for general toroidal geometry. Initial results are presented from the PENT code developed in tandem with IPEC, and comparisons with previous approximate methods show that the physics retained within the generalized results is important at experimentally relevant aspect ratio and shaping. Especially, the PENT calculation is shown to recover predicted behaviors in superbanana plateau regime with improved accuracy.

The PENT code is a fast, single-processor tool for computing the torque from nonambipolar transport in perturbed equilibria across kinetic regimes by including general geometric effects. This is important, as tokamak plasmas often span multiple regimes and have strong shaping in practice. The SBP limit in particular can be significant, since ITER may operate largely in this regime. Like most modern tokamaks, ITER will also have strong plasma shaping that will affect the BHR conditions and through them the ultimate value of the NTV torque. The previous RLAR approximation was actively applied to present tokamak experiments^{6,31,33,38–40} but its role will be replaced by PENT, which will offer a computationally inexpensive calculation of the toroidal torque in broader experimental conditions up to ITER-relevant regime.

ACKNOWLEDGMENTS

This research was supported by the U.S. Department of Energy under Contract DE-AC02-09CH11466 with Princeton Plasma Physics Laboratory, and in part by the Department of Energy Office of Science Graduate Fellowship Program (DOE SCGF), made possible in part by the American Recovery and Reinvestment Act of 2009, administered by ORISE-ORAU under Contract DE-AC05-06OR23100. Author N.C. Logan would like to thank J.E. Menard and E.J. Strait for providing insight and support throughout this work.

REFERENCES

- ¹K. C. Shaing, *Phys. Fluids* **26**, 3315 (1983).
- ²S. P. Hirshman, K. C. Shaing, W. I. van Rij, C. O. Beasley, and E. C. Crume, *Phys. Fluids* **29**, 2951 (1986).

- ³W. Zhu et al., Phys. Rev. Lett. **96** (2006).
- ⁴A. M. Garofalo et al., Phys. Rev. Lett. **101**, 1 (2008).
- ⁵A. J. Cole et al., Phys. Plasmas **18**, 055711 (2011).
- ⁶K. H. Burrell et al., Phys. Plasmas **19**, 056117 (2012).
- ⁷J. R. Cary and S. G. Shasharina, Phys. Plasmas **4**, 3323 (1997).
- ⁸A. J. Cole et al., Phys. Rev. Lett. **106**, 1 (2011).
- ⁹K. C. Shaing, S. A. Sabbagh, and M. S. Chu, Nucl. Fusion **50**, 025022 (2010).
- ¹⁰J.-K. Park, A. H. Boozer, and J. E. Menard, Phys. Rev. Lett. **102**, 1 (2009).
- ¹¹J.-K. Park, A. H. Boozer, and A. H. Glasser, Phys. Plasmas **14**, 052110 (2007).
- ¹²A. H. Glasser and M. S. Chance, Bull. Am. Phys. Soc. **42**, 1848 (1997).
- ¹³J.-K. Park, Phys. Plasmas **18**, 110702 (2011).
- ¹⁴J. D. Callen, Nucl. Fusion **51**, 094026 (2011).
- ¹⁵A. H. Boozer, Phys. Plasmas **16**, 52505 (2009).
- ¹⁶R. J. Goldston and P. P. H. Rutherford, *Introduction to Plasma Physics*, Taylor & Francis, 1995.
- ¹⁷A. Clebsch, J. Reine Angew. Math. **56** (1859).
- ¹⁸A. H. Boozer, Rev. Mod. Phys. **76**, 1071 (2005).
- ¹⁹F. Hinton and R. Hazeltine, Rev. Mod. Phys. **48**, 239 (1976).
- ²⁰A. H. Boozer, Phys. Fluids **23**, 2283 (1980).
- ²¹K. C. Shaing, S. A. Sabbagh, and M. S. Chu, Plasma Phys. Control. Fusion **51**, 35009 (2008).
- ²²B. Hu, R. Betti, and J. Manickam, Phys. Plasmas (2005).
- ²³Y. Liu, M. S. Chu, I. T. Chapman, and T. C. Hender, Phys. Plasmas **15**, 112503 (2008).
- ²⁴Y. Liu et al., Plasma Phys. Control. Fusion **52**, 104002 (2010).
- ²⁵J. W. Berkery et al., Phys. Plasmas **17**, 082504 (2010).
- ²⁶J. W. Berkery et al., Phys. Rev. Lett. **104**, 035003 (2010).
- ²⁷I. T. Chapman, S. E. Sharapov, G. T. a. Huysmans, and a. B. Mikhailovskii, Phys. Plasmas **13**, 062511 (2006).
- ²⁸L. Solov'ev, Sov. Phys. JETP (1968).
- ²⁹M. S. Chance et al., J. Comput. Phys. **28**, 1 (1978).
- ³⁰K. Kim, J.-K. Park, G. J. Kramer, and A. H. Boozer, Phys. Plasmas **19**, 82503 (2012).
- ³¹J.-K. Park et al., Phys. Rev. Lett. **111**, 095002 (2013).

- ³²S. Satake, J.-K. Park, H. Sugama, and R. Kanno, Phys. Rev. Lett. **107**, 55001 (2011).
- ³³A. M. Garofalo et al., Nucl. Fusion **51**, 083018 (2011).
- ³⁴K. Kim, J.-K. Park, and A. H. Boozer, Phys. Rev. Lett. **110**, 185004 (2013).
- ³⁵A. Galeev and R. Sagdeev, Sov. Phys. JETP **26**, 233 (1968).
- ³⁶A. A. Galeev, R. Z. Sagdeev, H. Furth, and M. Rosenboth, Phys. Rev. Lett. **22**, 511 (1969).
- ³⁷K. C. Shaing, Phys. Plasmas **10**, 1443 (2003).
- ³⁸J.-K. Park, A. H. Boozer, J. E. Menard, S. P. Gerhardt, and S. A. Sabbagh, Phys. Plasmas **16**, 082512 (2009).
- ³⁹J.-K. Park et al., Phys. Plasmas **16**, 056115 (2009).
- ⁴⁰S. P. Gerhardt et al., Plasma Phys. Control. Fusion **52**, 104003 (2010).

The Princeton Plasma Physics Laboratory is operated
by Princeton University under contract
with the U.S. Department of Energy.

Information Services
Princeton Plasma Physics Laboratory
P.O. Box 451
Princeton, NJ 08543

Phone: 609-243-2245
Fax: 609-243-2751
e-mail: pppl_info@pppl.gov
Internet Address: <http://www.pppl.gov>